INTERNATIONAL JOURNAL OF NUMERICAL MODELLING: ELECTRONIC NETWORKS, DEVICES AND FIELDS
Int. J. Numer. Model. 2012; **25**:587–598
Published online 6 February 2012 in Wiley Online Library (wileyonlinelibrary.com). DOI: 10.1002/jnm.845

Fourth-order finite-difference time-domain method based on error-controlling concepts

Theodoros T. Zygiridis*,†

Department of Informatics and Telecommunications Engineering, University of Western Macedonia, Karamanli and Lygeris, 50100 Kozani, Greece

SUMMARY

Conventional finite-difference time-domain (FDTD) methodologies incorporate discrete operators with the smallest truncation errors, as those are determined from the application of Taylor expansions. It is generally accepted that such choices, although quite efficient, do not necessarily provide optimum solutions when simulating electromagnetic wave phenomena. With the aim at improving accuracy without increasing the involved computational burden, the present paper is concerned with the development of a higher-order FDTD algorithm, which, in contrast to classic trends, is primarily based on the application of error-controlling ideas to its difference approximations. In essence, a fourth-order scheme is presented, whose spatial expressions are designed to remedy the leading terms of suitable error formulae. The latter can be easily extracted for each operator, given that the general nature of the expected solutions is known in advance. A correction factor is next added to the temporal operators to compensate for remaining errors at a selected wavelength. Unlike other approaches with single-frequency optimization, our technique is not strictly narrowband but capable of outperforming the conventional fourth-order FDTD algorithm in wideband simulations as well, without further modifications. The properties of the proposed scheme are verified through theoretical studies, as well as harmonic and multifrequency numerical tests, where comparisons with other standard techniques are performed. Copyright © 2012 John Wiley & Sons, Ltd.

Received 31 July 2011; Accepted 8 November 2011

KEY WORDS: finite-difference time-domain (FDTD) method; numerical dispersion; higher-order methods; error control

1. INTRODUCTION

In the context of time-domain electromagnetics and especially the study of wave-propagation phenomena, Yee's finite-difference time-domain (FDTD) algorithm [1,2] constitutes a popular researchers' choice, as it offers reasonable levels of accuracy, explicit equation updating, and relatively low computational complexity. On the other hand, with numerous contemporary applications in mind, it is clear that there exist several problems where the second-order accuracy of the standard FDTD method is simply not adequate. For instance, when performing large-scale simulations, the imprecise value of the numerical wave speed, which depends on frequency and direction of propagation, is translated into nonphysical phase discrepancies, thus degrading the reliability of the computations. In order to enhance discretization accuracy, various high-order implementations of space and/or time approximations have been proposed [3]. Although the corresponding operators and integrators seem to be more computationally intensive (e.g., an explicit fourth-order approximation of first derivatives requires four samples, whereas second-order operators only two), they are proven more efficient than low-order counterparts in practice, as they provide better error-to-cost ratios.

*Correspondence to: Theodoros T. Zygiridis, Department of Informatics and Telecommunications Engineering, University of Western Macedonia, Karamanli and Lygeris, 50100 Kozani, Greece.
†E-mail: tzygiridis@uowm.gr

A common feature of the aforementioned (low and high order) schemes is their adoption of the so-called standard finite differencing, which produces approximate operators with the smallest possible truncation errors. This property ensures the convergence of the calculated solutions to the exact one, when discretization density is increased (or when very low frequencies are considered). Nevertheless, this classic approach seems to be more generic than necessary, as it overlooks the nature of the problem's expected solutions (combinations of waves, in our case). Hence, obtaining optimal solutions for a given level of computational complexity is a task with no obvious solution. Experience has shown that preserving a high-order truncation error is not a necessary condition if highly accurate computations are required. In essence, amended modeling of high-frequency components (which are, in general, more susceptible to numerical dispersion than the ones at lower frequencies) can be beneficial, even if it occurs at the expense of the performance at longer wavelengths. Such ideas have become quite popular during the previous years. In fact, they have triggered a growing interest in the development of computational algorithms that do not rely on conventional practices, yet are capable of improving simulation conditions significantly.

Knowing the general characteristics of the anticipated solutions has been exploited for the construction of finite-difference techniques, which essentially attempt to preserve the exact dispersion relation at the discrete level. Toward this direction, one of the first approaches included the optimization of the numerical wavenumber over the desired frequency range or the combination of this technique with truncated Taylor series approximations [4]. Another example is the nonstandard FDTD method, which introduces multidimensional spatial stencils and relies on the manipulation of an error expression to derive an isotropic Laplacian [5]. Advanced FDTD algorithms have been designed after introducing—and effectively minimizing—space-time error functions [6,7], which originate from assuming plane wave solutions. Sets of local approximations emanating from knowing specific features of the investigated problem are used in [8] for defining finite-difference schemes with increased reliability while remaining simple to implement. The idea of spectral order of accuracy, which combines the formal order of accuracy with the concept of numerical dispersion, is introduced in [9] and exploited for the development of various schemes for the wave equation. Single-frequency minimization of the dispersion error is accomplished in [10] by introducing scaling (for the material parameters) and weighting (for the discrete operators) factors, calculated with the aid of the numerical dispersion relation and other optimization methods. With the aim at the discretization of the acoustic wave equation, plane-wave theory is used in [11] for the construction of a finite-difference methodology, which is proven more superior than the conventional approach, even though the pertinent computational cost is not modified. Despite the variety of the fundamental concepts, it is evident that the aforementioned examples demonstrate the possibility of producing highly accurate schemes, avoiding the limitations set by conventional trends.

In this paper, we develop a 2D high-order FDTD scheme, whose finite-difference operators are constructed by exploiting error-controlling concepts, rather than pursuing the minimization of the corresponding truncation errors. The update equations of the proposed method are similar to those of the fourth-order FDTD algorithm, which embodies a high-order leapfrog integrator [12]. The realization of the latter entails the computation of third-order spatial derivatives, avoiding the storage of field values at more than one time levels. For conventional expressions to be avoided, error functions are formulated for each spatial approximation after assuming plane-wave forms for field components. The discrete operators initially introduce some unknown coefficients, which are then computed, so that rectified errors are produced in an isotropic fashion. It is noted that these factors can be found in closed form, thus facilitating the in-depth investigation of the scheme's properties. A slight correction is subsequently applied to the remaining temporal operator, for balancing the—already lower—spatial flaws. We verify that the proposed technique presents an error minimum at a chosen frequency point, yet it is not a strictly narrowband method, as it preserves nontrivial wideband characteristics. The latter are also pointed out theoretically by computing the numerical phase velocity from the numerical dispersion relation. It is shown that fourth-order convergence is accomplished by the examined technique, albeit Taylor expansions are completely avoided. Because the optimized algorithm does not alter the structure of the fourth-order method, both techniques introduce identical computation burden. Finally, a number of numerical simulations are performed so that the theoretical findings are validated.

DOI: 10.1002/jnm

2. FDTD ALGORITHM BASED ON ERROR-CONTROLLING CONCEPTS

In the following paragraphs, we are concerned with the approximate solution of the 2D lossless Maxwell's equations

$$\begin{cases} \varepsilon \dfrac{\partial E_x}{\partial t} = \dfrac{\partial H_z}{\partial y} \\ \varepsilon \dfrac{\partial E_y}{\partial t} = -\dfrac{\partial H_z}{\partial x} \\ \mu \dfrac{\partial H_z}{\partial t} = \dfrac{\partial E_x}{\partial y} - \dfrac{\partial E_y}{\partial x}, \end{cases} \tag{1}$$

where ε and μ are the permittivity and permeability of the material filling the space. We assume spatial discretization with Δx, Δy steps, and time-step size equal to Δt. First, we briefly describe the fourth-order FDTD scheme (hereafter referred to as the 'standard (4,4) method'), which will provide the framework for the new technique.

2.1. The standard fourth-order FDTD method

An extension of Yee's method to a fourth-order accurate scheme in both space and time is accomplished by replacing the second-order operators with high-order counterparts. If $u_{i,j}$ denotes the value of component $u(x, y, t)$ at position $(i\,\Delta x, j, \Delta y)$, differentiation in space is conducted with the formulae

$$\mathrm{D}_x^{(4)} u_{i,j} = \frac{9}{8\Delta x}\left(u_{i+\frac{1}{2},j} - u_{i-\frac{1}{2},j}\right) - \frac{1}{24\Delta x}\left(u_{i+\frac{3}{2},j} - u_{i-\frac{3}{2},j}\right) \tag{2}$$

$$\mathrm{D}_y^{(4)} u_{i,j} = \frac{9}{8\Delta y}\left(u_{i,j+\frac{1}{2}} - u_{i,j-\frac{1}{2}}\right) - \frac{1}{24\Delta y}\left(u_{i,j+\frac{3}{2}} - u_{i,j-\frac{3}{2}}\right). \tag{3}$$

On the other hand, a fourth-order approximation for time derivatives can be obtained from combining Taylor expansions and has the form

$$\mathrm{D}_t^{(4)} u^n = \mathrm{D}_t^{(2)} u^n - \frac{\Delta t^2}{24}\frac{\partial^3 u}{\partial t^3}, \tag{4}$$

where

$$\mathrm{D}_t^{(2)} u^n = \frac{u^{n+\frac{1}{2}} - u^{n-\frac{1}{2}}}{\Delta t} \tag{5}$$

is the usual second-order expression and u^n is the value of $u(x, y, t)$ at time instant $n\,\Delta t$. Direct discretization of the third-order derivative may augment memory requirement and possibly raise unwanted stability issues. To avoid these phenomena, we express $\partial^3/\partial t^3$ with the aid of spatial derivatives:

$$\frac{\partial^3}{\partial t^3}\begin{bmatrix} E_x \\ E_y \\ H_z \end{bmatrix} = \begin{bmatrix} 0 & 0 & \dfrac{c_0^2}{\varepsilon}\left(\dfrac{\partial^3}{\partial y^3} + \dfrac{\partial^3}{\partial x^2 \partial y}\right) \\ 0 & 0 & -\dfrac{c_0^2}{\varepsilon}\left(\dfrac{\partial^3}{\partial x^3} + \dfrac{\partial^3}{\partial y^2 \partial x}\right) \\ \dfrac{c_0^2}{\mu}\left(\dfrac{\partial^3}{\partial y^3} + \dfrac{\partial^3}{\partial x^2 \partial y}\right) & -\dfrac{c_0^2}{\mu}\left(\dfrac{\partial^3}{\partial x^3} + \dfrac{\partial^3}{\partial y^2 \partial x}\right) & 0 \end{bmatrix} \begin{bmatrix} E_x \\ E_y \\ H_z \end{bmatrix}, \tag{6}$$

where $c_0 = 1/\sqrt{\mu\varepsilon}$ is the free-space speed of light. Fourth-order accuracy is maintained, even if the higher derivatives are discretized with second-order expressions, for example,

$$\mathrm{D}_{xxx}^{(2)} u_{i,j} = \frac{1}{\Delta x^3}\left[u_{i+\frac{3}{2},j} - u_{i-\frac{3}{2},j} - 3\left(u_{i+\frac{1}{2},j} - u_{i-\frac{1}{2},j}\right)\right] \tag{7}$$

$$\mathrm{D}_{yyx}^{(2)} u_{i,j} = \frac{1}{\Delta y^2 \Delta x}\left[u_{i+\frac{1}{2}j+1} - u_{i-\frac{1}{2},j+1} + u_{i+\frac{1}{2},j-1} - u_{i-\frac{1}{2},j-1} - 2\left(u_{i+\frac{1}{2},j} - u_{i-\frac{1}{2},j}\right)\right] \tag{8}$$

Operators $\mathrm{D}_{yyy}^{(2)}$ and $\mathrm{D}_{xxy}^{(2)}$ are defined in a similar manner. Consequently, despite the use of the more sophisticated time integration, only the $\mathrm{D}_t^{(2)}$ temporal operator appears in the update equations. This means that the structure of the (4,4) scheme resembles that of Yee's algorithm, especially if transition from continuous to discrete state is described by the following substitutions:

DOI: 10.1002/jnm

$$\frac{\partial}{\partial x} \to \mathrm{D}_x^{(4)} + \frac{(c_0\Delta t)^2}{24}\left(\mathrm{D}_{xxx}^{(2)} + \mathrm{D}_{yyx}^{(2)}\right)$$
$$\frac{\partial}{\partial y} \to \mathrm{D}_y^{(4)} + \frac{(c_0\Delta t)^2}{24}\left(\mathrm{D}_{yyy}^{(2)} + \mathrm{D}_{xxy}^{(2)}\right)$$
$$\frac{\partial}{\partial t} \to \mathrm{D}_t^{(2)}$$

2.2. Application of error control

Instead of minimizing the truncated terms of the finite-difference operations, as those emerge from the corresponding Taylor series, consistent error expressions can be obtained by taking into account that solutions are expected to have the form of propagating waves. By comparing the actions of exact and approximating operators on suitable functions, reliable error estimation is conducted and operators that control their discretization performance can be designed. For first-order spatial differentiation, the following four-point operators are selected:

$$\mathrm{D}_x u_{i,j} = \frac{C_1^x\left(u_{i+\frac{1}{2},j} - u_{i-\frac{1}{2},j}\right) + C_2^x\left(u_{i+\frac{3}{2},j} - u_{i-\frac{3}{2},j}\right)}{\Delta x} \tag{9}$$

$$\mathrm{D}_y u_{i,j} = \frac{C_1^y\left(u_{i,j+\frac{1}{2}} - u_{i,j-\frac{1}{2}}\right) + C_2^y\left(u_{i,j+\frac{3}{2}} - u_{i,j-\frac{3}{2}}\right)}{\Delta y}, \tag{10}$$

whereas the following schemes are introduced for the third-order derivatives:

$$\mathrm{D}_{xxx} u_{i,j} = \frac{D_1^x\left(u_{i+\frac{1}{2},j} - u_{i-\frac{1}{2},j}\right) + D_2^x\left(u_{i+\frac{3}{2},j} - u_{i-\frac{3}{2},j}\right)}{\Delta x^3} \tag{11}$$

$$\mathrm{D}_{yyy} u_{i,j} = \frac{D_1^y\left(u_{i,j+\frac{1}{2}} - u_{i,j-\frac{1}{2}}\right) + D_2^y\left(u_{i,j+\frac{3}{2}} - u_{i,j-\frac{3}{2}}\right)}{\Delta y^3}. \tag{12}$$

The formulae used for mixed derivatives have the following form:

$$\mathrm{D}_x u_{i,j} = \frac{E_1^x\left(u_{i+\frac{1}{2},j} - u_{i-\frac{1}{2},j}\right) + E_2^x\left(u_{i+\frac{1}{2},j+1} - u_{i-\frac{1}{2},j+1} + u_{i+\frac{1}{2},j-1} - u_{i-\frac{1}{2},j-1}\right)}{\Delta y^2 \Delta x} \tag{13}$$

$$\mathrm{D}_{xxy} u_{i,j} = \frac{E_1^y\left(u_{i,j+\frac{1}{2}} - u_{i,j-\frac{1}{2}}\right) + E_2^y\left(u_{i+1,j+\frac{1}{2}} - u_{i+1,j-\frac{1}{2}} + u_{i-1,j+\frac{1}{2}} - u_{i-1,j-\frac{1}{2}}\right)}{\Delta x^2 \Delta y}. \tag{14}$$

Evidently, Equations (9)–(14) are parametric generalizations of the counterparts incorporated by the standard (4,4) method. The error pertinent to each approximation can be estimated when applied to the test function $e^{-\mathrm{j}\mathbf{kr}}$, where $\mathbf{k} = k(\cos\phi\ \hat{\mathbf{x}} + \sin\phi\ \hat{\mathbf{y}})$, $k = \omega/c_0$ is the wavenumber, ϕ denotes propagation angles, and $\mathrm{j} = \sqrt{-1}$. For simplicity, only half of the operators are presented; the other ones are defined symmetrically. In the case of the D_x operator, we have

$$\left(\mathrm{D}_x - \frac{\partial}{\partial x}\right)e^{-\mathrm{j}\mathbf{kr}} = \frac{-2\mathrm{j}}{\Delta x}\sum_{i=1}^{2} C_i^x \sin\left(\frac{2i-1}{2} k\cos\phi\,\Delta x\right) + \mathrm{j}k\cos\phi. \tag{15}$$

To facilitate uniform—with respect to ϕ—error annihilation and, hence, coefficient values that do not depend on the direction of propagation, we obtain the corresponding trigonometric series:

$$\left(\mathrm{D}_x - \frac{\partial}{\partial x}\right)e^{-\mathrm{j}\mathbf{kr}} = \frac{-4\mathrm{j}}{\Delta x}\sum_{i=1}^{2} C_i^x \sum_{n=0}^{\infty}(-1)^n J_{2n+1}\left(\frac{2i-1}{2} k\Delta x\right)\cos[(2n+1)\phi] + \mathrm{j}k\cos\phi \tag{16}$$

where J_n denotes nth order Bessel functions of the first kind. The vanishing of the first two terms in Equation (16) (which correspond to $\cos\phi$ and $\cos 3\phi$) leads to two equations, and the coefficients C_1^x and C_2^x are determined from the system

DOI: 10.1002/jnm

$$\begin{bmatrix} J_1\left(\frac{k\Delta x}{2}\right) & J_1\left(\frac{3k\Delta x}{2}\right) \\ J_3\left(\frac{k\Delta x}{2}\right) & J_3\left(\frac{3k\Delta x}{2}\right) \end{bmatrix} \quad \begin{bmatrix} C_1^x \\ C_2^x \end{bmatrix} = \begin{bmatrix} \frac{k\Delta x}{4} \\ 0 \end{bmatrix}. \tag{17}$$

The previously calculated parameters asymptotically obtain the values of the standard fourth-order operator, as it is $C_1^x \simeq \frac{9}{8} + \frac{9}{512}(k\Delta x)^2$ and $C_2^x \simeq -\frac{1}{24} - \frac{3}{512}(k\Delta x)^2$.

The same procedure can be applied for the higher derivatives. In the case of D_{xxx}, the error is described by

$$\left(\mathrm{D}_{xxx} - \frac{\partial^3}{\partial x^3}\right) e^{-\mathrm{j}\mathbf{kr}} = -\frac{2\mathrm{j}}{\Delta x^3} \sum_{i=1}^{2} D_i^x \sin\left(\frac{2i-1}{2} k\cos\phi\Delta x\right) - \mathrm{j}k^3\cos^3\phi \tag{18}$$

and the necessary expansion has the form

$$\begin{aligned} \left(\mathrm{D}_{xxx} - \frac{\partial^3}{\partial x^3}\right) e^{-\mathrm{j}\mathbf{kr}} = &-\frac{4\mathrm{j}}{\Delta x^3} \sum_{i=1}^{2} D_i^x \sum_{n=0}^{\infty} (-1)^n J_{2n+1}\left(\frac{2i-1}{2} k\Delta x\right) \cos[(2n+,1)\phi] \\ &-\frac{1}{4}\mathrm{j}k^3(3\cos\phi + \cos 3\phi) \end{aligned} \tag{19}$$

Then, an accurate version of the operator is defined by selecting its parameters according to the equations

$$\begin{bmatrix} -J_1\left(\frac{k\Delta x}{2}\right) & -J_1\left(\frac{3k\Delta x}{2}\right) \\ J_3\left(\frac{k\Delta x}{2}\right) & J_3\left(\frac{3k\Delta x}{2}\right) \end{bmatrix} \quad \begin{bmatrix} D_1^x \\ D_2^x \end{bmatrix} = \frac{1}{16}(k\Delta x)^3 \begin{bmatrix} 3 \\ 1 \end{bmatrix}. \tag{20}$$

As previously discussed, these constants obtain specific values when $\Delta x \to 0$, as we find $D_1^x \simeq -3 - \frac{15}{32}(k\Delta x)^2$ and $D_2^x \simeq 1 + \frac{5}{32}(k\Delta x)^2$.

Finally, let us consider the D_{yyx} operator. The corresponding error formula is

$$\begin{aligned} \left(\mathrm{D}_{yyx} - \frac{\partial^3}{\partial y^2 \partial x}\right) e^{-\mathrm{j}\mathbf{kr}} = &\frac{-2\mathrm{j}}{\Delta x \Delta y^2} \left[E_1^x \sin\left(\frac{1}{2} k\cos\phi\Delta x\right) \right. \\ &\left. + 2E_2^x \sin\left(\frac{1}{2} k\cos\phi\Delta x\right) \cos(k\sin\phi\Delta y) \right] - \mathrm{j}k^3\cos\phi\sin^2\phi, \end{aligned} \tag{21}$$

and the trigonometric series has the form

$$\begin{aligned} \left(\mathrm{D}_{yyx} - \frac{\partial^3}{\partial y^2 \partial x}\right) e^{-j\mathbf{kr}} = &-\frac{4\mathrm{j}}{\Delta x \Delta y^2} \left[E_1^x \sum_{n=0}^{\infty} (-1)^n J_{2n+1}\left(\frac{1}{2} k\Delta x\right) \cos[(2n+1)\phi] \right. \\ &\left. + 2E_2^x \sum_{n=0}^{\infty} (-1)^n J_{2n+1}(\kappa) \cos[(2n+1)\phi_0] \cos[(2n+1)\phi] \right] \\ &-\frac{1}{4}\mathrm{j}k^3(\cos\phi - \cos 3\phi). \end{aligned} \tag{22}$$

where $\kappa = k\sqrt{\Delta x^2/4 + \Delta y^2}$ and $\phi_0 = \arctan(2\Delta y/\Delta x)$. The optimum coefficients are now produced from

$$\begin{bmatrix} -J_1\left(\frac{1}{2}k\Delta x\right) & -2J_1(\kappa)\cos\phi_0 \\ J_3\left(\frac{1}{2}k\Delta x\right) & 2J_3(\kappa)\cos 3\phi_0 \end{bmatrix} \quad \begin{bmatrix} E_1^x \\ E_2^x \end{bmatrix} = \frac{1}{16}k^3\Delta x\Delta y^2 \begin{bmatrix} 1 \\ -1 \end{bmatrix}. \tag{23}$$

In agreement with Equation (8), the asymptotic behavior of these variables is described by $E_1^x \simeq -2 - \frac{7}{48}(k\Delta x)^2$ and $E_2^x \simeq 1 + \frac{7}{96}(k\Delta x)^2$ when $\Delta y = \Delta x$.

DOI: 10.1002/jnm

In a similar sense, temporal derivatives are approximated with a parametric form as well:

$$\mathrm{D}_t u^n = C_t \frac{u^{n+\frac{1}{2}} - u^{n-\frac{1}{2}}}{\Delta t}. \tag{24}$$

To determine C_t, we follow a different approach. Rather than to separately minimize the time-related inaccuracies, our goal is to attempt the elimination of the remaining error from the spatial operations. Naturally, this error is anisotropic and cannot disappear completely, unless an angular-dependent—yet, non-applicable—C_t is selected. This can be avoided by utilizing its mean value, especially if one takes into account that numerical anisotropy is, in any case, already reduced because of the optimized coefficients. Toward this direction, the numerical dispersion relation of the scheme plays an important role and can be compactly expressed as

$$C_t^2 \mathrm{T}^2(\omega) = \mathrm{X}^2\left(\tilde{k}\right) + \mathrm{Y}^2\left(\tilde{k}\right), \tag{25}$$

where

$$\mathrm{T}(\omega) = \frac{2\mathrm{j}}{c_0 \Delta t} \sin\left(\frac{\omega \Delta t}{2}\right) \tag{26}$$

$$\begin{aligned} \mathrm{X}(k) = &-\frac{2\mathrm{j}}{\Delta x} \sum_{i=1}^{2} C_i^x \sin\left(\frac{2i-1}{2} k_x \Delta x\right) - \frac{2\mathrm{j}}{\Delta x} \frac{(c_0 \Delta t)^2}{24} \left\{ \frac{1}{\Delta x^2} \sum_{i=1}^{2} D_i^x \sin\left(\frac{2i-1}{2} k_x \Delta x\right) \right. \\ &\left. + \frac{1}{\Delta y^2} \left[E_1^x + 2E_2^x \cos\left(k_y \Delta y\right)\right] \sin\left(\frac{1}{2} k_x \Delta x\right) \right\} \end{aligned} \tag{27}$$

$$\begin{aligned} \mathrm{Y}(k) = &-\frac{2\mathrm{j}}{\Delta y} \sum_{i=1}^{2} C_i^x \sin\left(\frac{2i-1}{2} k_y \Delta y\right) - \frac{2\mathrm{j}}{\Delta y} \frac{(c_0 \Delta t)^2}{24} \left\{ \frac{1}{\Delta y^2} \sum_{i=1}^{2} D_i^y \sin\left(\frac{2i-1}{2} k_y \Delta y\right) \right. \\ &\left. + \frac{1}{\Delta x^2} \left[E_1^y + 2E_2^y \cos(k_x \Delta x)\right] \sin\left(\frac{1}{2} k_y \Delta y\right) \right\} \end{aligned} \tag{28}$$

and $\tilde{k}$ is the numerical wavenumber. An angle-dependent value for C_t can be obtained from Equation (25) provided that we set $\tilde{k} = k = \omega / c_0$ as a means of enforcing algorithmic reliability. For the reasons mentioned previously, its mean value is used instead. In other words, we select

$$C_t = \frac{1}{\mathrm{T}(\omega)} \sqrt{\frac{1}{2\pi} \int_0^{2\pi} \left[\mathrm{X}^2(k) + \mathrm{Y}^2(k)\right] \, \mathrm{d}\phi}.$$

Evidently, all the calculated coefficients depend on frequency. In practice, for the more complicated implementation of frequency-dependent parameters (e.g., [6]) to be avoided, a design frequency is selected according to criteria pertinent to the problem under study (e.g., the spectral content of the excitation schemes). For reference, Table I presents the calculated coefficients for various optimization frequencies, expressed as a function of the cell size in terms of the wavelength. In this case, we consider $\Delta x = \Delta y = \Delta$, which produces $C_i^x = C_i^y$, $D_i^x = D_i^y$, and $E_i^x = E_i^y$ for $i = 1, 2$. As seen, the temporal coefficient C_t quickly obtains a value close to 1. This fact verifies that the proposed spatial

Table I. Coefficients values for various optimization points when $\Delta x = \Delta y = \Delta$ (maximum time steps are considered).

	$\Delta = \lambda/10$	$\Delta = \lambda/20$	$\Delta = \lambda/40$	$\Delta = \lambda/80$
$C_1^{x,y}$	1.13193929	1.12673497	1.12543374	1.12510844
$C_2^{x,y}$	−0.04405811	−0.04224978	−0.04181155	−0.04170283
$D_1^{x,y}$	−3.18545810	−3.04629152	−3.01156813	−3.00289173
$D_2^{x,y}$	1.06391494	1.01555837	1.00386399	1.00096441
$E_1^{x,y}$	−2.05816487	−2.01443054	−2.00360076	−2.00089976
$E_2^{x,y}$	1.02929031	1.00722803	1.00180117	1.00044993
C_t	0.99997956	0.99999873	0.99999992	0.99999999

DOI: 10.1002/jnm

approximations introduce only a small amount of remaining error; thus, only a slight correction is actually required to ensure the desired balancing. In fact, this evidence indicates that C_t converges to 1 at a fourth-order rate with respect to the cell size in contrast to the coefficients of the spatial operators.

Regarding the stability of the algorithm, we have found that a value of the time step that guarantees stability in the case of equal spatial steps ($\Delta x = \Delta y = \Delta$) should satisfy the inequality

$$\frac{\sqrt{2}c_0\Delta t}{\Delta} \leq \left[C_1 - C_2 + \frac{(c_0\Delta t)^2}{24\Delta^2}(D_1 - D_2 + E_1 - 2E_2) \right]^{-1}. \tag{29}$$

In practice, time steps that comply with Equation (29) are practically the same as that of the standard (4,4) and Yee's algorithms. Therefore, the execution of stable simulations by the new methodology does not entail any change of the computational cost compared with the standard (4,4) scheme.

3. PERFORMANCE ANALYSIS

Our first priority is to verify that the proposed approach of treating the error of each spatial operator separately results in accuracy improvement at the selected frequency point. For instance, consider the case where $\Delta x = \Delta y = \Delta = \lambda/10$. Figure 1 displays the relative error $|(\tilde{c} - c_0)/c_0|$ pertinent to the numerical phase velocity $\tilde{c}$ in the case of Yee's algorithm, the standard (4,4) scheme, and the proposed scheme. It becomes apparent that our spatial error-controlling procedure, combined with the correction of temporal operators, leads to significant reduction of inaccuracies in an isotropic fashion. It should be clarified, though, that it is not our primary intention to accomplish maximum error cancellation only at the selected wavelength because single-frequency optimization may eventually lead to very narrowband performance (e.g., [5]).

In gaining further insight, the overall error, defined at a specific frequency as

$$e_c = \frac{1}{2\pi}\int_0^{2\pi} \left| 1 - \frac{\tilde{c}}{c_0} \right| \mathrm{d}\phi, \tag{30}$$

is plotted as a function of the cell size in Figure 2. For the new method, optimization is performed at each point of the horizontal axis. The results from the standard (2, 4) approach, which is second-order accurate in time and fourth-order accurate in space, are also shown for comparison. The data of Figure 2 verify the validity of the proposed optimization scheme, irrespective of the chosen optimization point. In fact, it is concluded that at least at the design frequency, the error reduces at a fourth-order rate, despite the fact that no special care for the order of the truncated terms has been taken. When considering the maximum allowable time step, the level of improvement reaches a factor of more than 20, compared with the (4,4) method, and more than 700, with respect to the (2, 4) technique. The latter attains fourth-order convergence despite its low-order temporal accuracy because the time step does not change linearly with Δ but is selected equal to $0.85\Delta/\left(nc_0\sqrt{2}\right)$ (n indicates the level of mesh refinement compared with the initial grid where $\Delta = \lambda/10$).

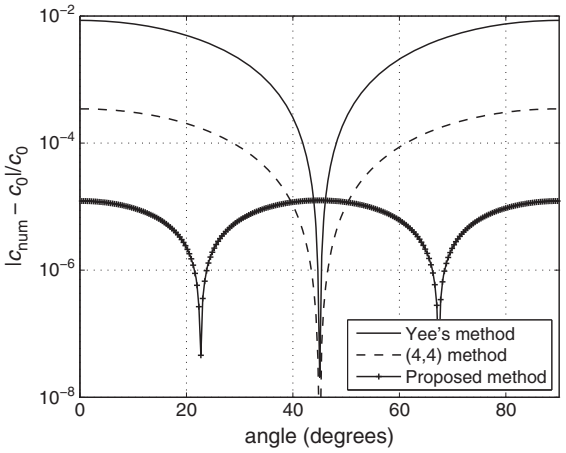

Figure 1. Relative error in the numerical phase velocity versus propagation angle.

DOI: 10.1002/jnm

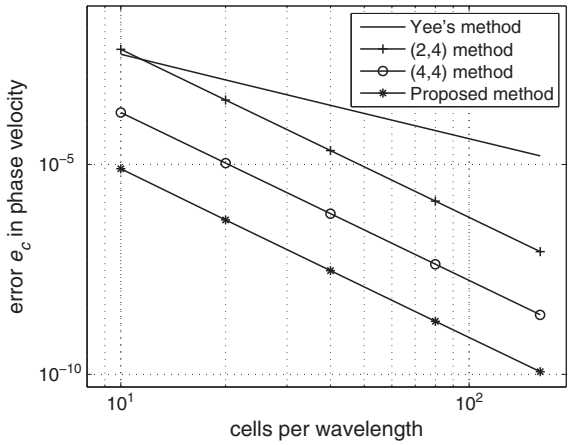

Figure 2. Overall error in the numerical phase velocity versus grid density. In the case of the proposed scheme, optimization is performed at each point of the horizontal axis.

The conclusion that the new scheme is fourth-order accurate at the design frequency can be verified from the scheme's dispersion relation as well if the latter is used as an error indicator. In doing that, it is required that $\tilde{k} = k$. For clarity, let us consider the standard (4,4) scheme first. In this case, if we choose $\Delta t = \frac{Q\Delta}{c_0}$, we obtain

$$\mathrm{T}^2_{(4,4)} - \mathrm{X}^2_{(4,4)} - \mathrm{Y}^2_{(4,4)} \simeq \frac{-8Q^4 + 60Q^2 - 45 + (20Q^2 - 27)\cos 4\phi}{30,720} k^6 \Delta x^4. \tag{31}$$

This result verifies the formal order of the scheme, as the term (31) is representative of the combined space-time errors. On the other hand, a similar expression can also be found for the proposed algorithm. Recall that C_t converges to 1 at a fourth-order rate, as we have concluded from Table I. This means that it can be written as $C_t = 1 + \alpha\Delta^4 + \ldots$. Then, we obtain

$$\mathrm{T}^2 - \mathrm{X}^2 - \mathrm{Y}^2 \simeq -\frac{\alpha}{2} k^2 \Delta x^4 + \frac{-48Q^4 + (40Q^2 - 27)\cos 4\phi}{184,320} k^6 \Delta x^4. \tag{32}$$

Therefore, the new scheme is also fourth-order accurate at the optimization point, as implied by Equation (32). The constant term involving α should not concern us, as it will be eventually cancelled by other similar ones, thanks to the selected value of C_t. If we choose $Q = 1/\sqrt{2}$, then in the case of the (4,4) technique, the angle-dependent term is $-(17/30,720)\cos 4\phi$, whereas it becomes $-(7/184,320)\cos 4\phi$ for the proposed technique.

Having verified the single-frequency response of the new algorithm, we turn our attention to the evaluation of its wideband characteristics. Figure 3 exhibits the calculated error curves for Yee's

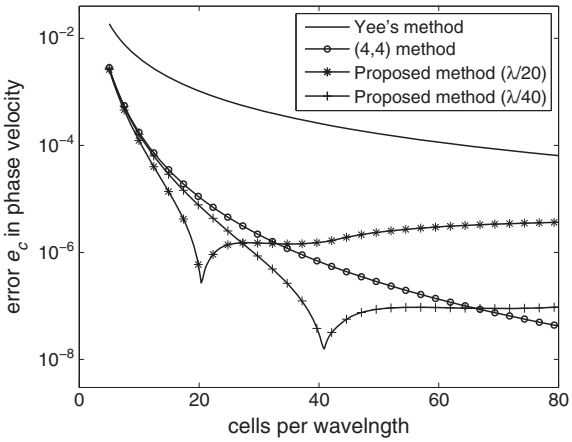

Figure 3. Overall error in phase velocity over an extended band of frequencies.

DOI: 10.1002/jnm

algorithm, the standard (4,4) method, and the proposed method, when the latter is optimized either at 20 or 40 cells per wavelength. It is easily deduced that the error curves of the new scheme attain a distinct minimum at the point of optimization. As seen, it is not as deep as in other cases, for example, [5]. This is not necessarily an undesirable feature because experience has shown that the more intense the error minimum, the more narrowband the overall performance. In the latter case, perhaps a different strategy should be followed, such as implementation of frequency-dependent coefficients [6], which inevitably leads to expansion of the spatial stencil. Our approach seems to be somewhere in the middle because it attains satisfactory wideband performance for all smaller wavelengths, as well as for a part of the longer ones. Consequently, selecting the design point according to the higher-frequency content of the simulated problem should suffice for better overall performance.

4. NUMERICAL RESULTS

In the first numerical test, we model a 7×4-cm rectangular cavity with perfectly conducting boundaries. The $TE_{2,2}$ mode is excited by enforcing the exact field distribution as initial condition throughout the computational domain. For errors due to incorrect boundary modeling to be avoided, the necessary symmetry conditions are utilized with the addition of external ghost nodes when calculating space derivatives close to the cavity's boundaries. Also, the standard (2,4) method is applied for comparison. In our case, the considered mesh sizes are $21n \times 12n$, $n = 1, 2, \ldots, 8$. The maximum time step is used for Yee's, (4,4), and proposed methods, whereas temporal discretization for the (2,4) scheme is dictated by time-step sizes equal to $0.85\Delta/\left(nc_0\sqrt{2}\right)$, for the reason mentioned previously. The produced L_2 error with respect to H_z is recorded during the simulations, whose duration corresponds to 2000 time steps in the case of the coarsest grid. Figure 4 depicts the maximum error values as a function of the corresponding spatial step. Evidently, the (2,4), the (4,4), and the proposed schemes outperform Yee's algorithm because of faster convergence. The optimized method provides better results than the conventional fourth-order scheme, thanks to the use of optimized operators. In this problem, the standard (4,4) scheme produces a more than 15-time larger error than the optimized counterpart. This practically means that the new scheme can attain the same accuracy with the standard (4,4) method, using a grid with half the density in both directions. For instance, the error of the (4,4) method is 2.48×10^{-5} when $\Delta = 0.556$ mm, whereas the proposed technique produces a comparable error of 2.56×10^{-5} with $\Delta = 1.111$ mm. The efficiency of the numerical schemes is also examined by plotting the produced error as a function of the necessary numerical time. The corresponding curves are drawn in Figure 5. It becomes apparent that the new method is more efficient than the standard (4,4), taking into account the fact that, for a given grid, the computational requirements are identical. The (2,4) scheme eventually becomes more efficient than Yee's algorithm, thanks to its convergence rate. However, owing to time-step restrictions, it cannot be as effective as the truly fourth-order methodologies. Consequently, the efficiency and superiority of the optimized approach is verified in this example.

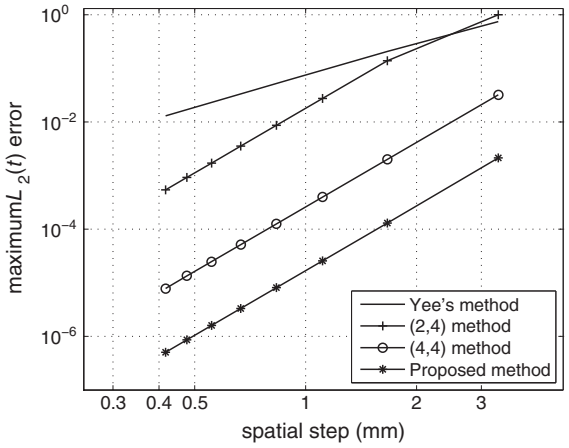

Figure 4. Error versus cell size in the cavity problem with one excited mode.

DOI: 10.1002/jnm

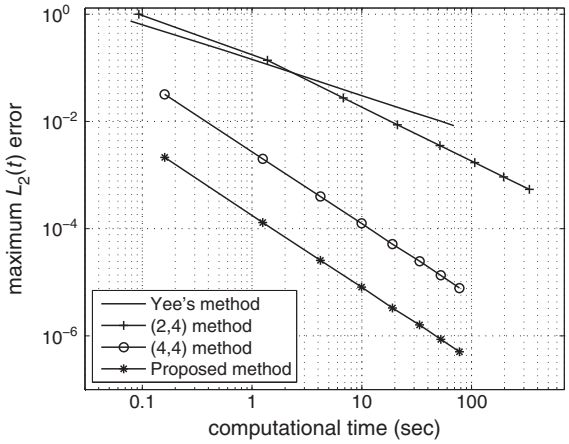

Figure 5. Error versus computational time in the cavity problem with one excited mode.

The following test considers a 4×40-cm parallel-plate waveguide, where the first three modes are excited at 4.5, 8.5, and 12 GHz. The electromagnetic field at the ports of the waveguide is prescribed at any time instant, according to the exact solution. The latter is used for implementing initial conditions throughout the computational domain as well. Four simulations are performed for each computational technique (Yee's, (4,4), and the proposed method), considering grids of $14n \times 140n$ cells, $n = 1, 2, 3, 4$ (excluding the buffer layers around the structure). In the case of the coarsest mesh, the simulations are conducted for 4000 time steps, equal to Yee's stability limit. The application of the new method is based on selecting the optimization frequency equal to the highest frequency component, that is, 12 GHz. The maximum L_2 errors are given in Table II, where we can safely conclude that fourth-order convergence rate is attained by the proposed algorithm in this wideband problem as well, despite the single-frequency optimization. Specifically, the new method produces errors that are at least an order of magnitude smaller than the standard (4,4) scheme; hence, its suitability for broadband simulations is confirmed.

In the final test, the first 20 modes of a 10×10-cm cavity with perfectly conducting boundaries are detected. Their exact resonant frequencies can be obtained analytically and are within the band 1.499–9.118 GHz. The computational domain is discretized with a 20×20 cell grid, whose resolution corresponds to 6.58 cells per wavelength at the highest frequency. All simulations are performed for 2^{17} time steps, yielding a frequency resolution of approximately 0.65 MHz. Field components are recorded at various positions at all time steps, and then the resonant frequencies are detected from the peaks of the Fourier transforms of the recorded waveforms. The differences between the exact frequencies and the calculated values are plotted in Figure 6. For the proposed scheme, the optimization frequency is selected either 6.5 or 7.5 GHz. As shown, both optimized schemes produce a lower overall error compared with the standard (4,4) approach. Specifically, the maximum absolute error for the (4,4) scheme is 15.6 MHz, which reduces to 7.29 and 4.67 MHz, respectively, for the two optimized implementations. In addition, the average value of the absolute errors for the (4,4) method is approximately 4 MHz, and this becomes 1.1 and 0.83 MHz for the optimized techniques. For reference, the Yee algorithm produces a maximum error of 172.8 MHz and a mean error of 40 MHz, thus pointing the superiority of the high-order solutions. These results are indicative of a fact that was pointed out in the Section 1. That is, improvement at high frequencies can be advantageous, even if it causes some loss of accuracy at low-frequency bands.

Table II. Maximum L_2 errors in the simulation of a parallel-plate waveguide supporting three propagating modes.

Δ (mm)	Yee	Rate	(4, 4)	Rate	Proposed	Rate
2.857	$4.35 \cdot 10^{-3}$	1.66	$3.26 \cdot 10^{-4}$	3.8	$1.83 \cdot 10^{-5}$	4.0
1.429	$1.19 \cdot 10^{-3}$		$2.49 \cdot 10^{-5}$		$1.16 \cdot 10^{-6}$	
0.952	$6.83 \cdot 10^{-4}$		$5.09 \cdot 10^{-6}$		$2.27 \cdot 10^{-7}$	
0.714	$4.29 \cdot 10^{-4}$		$1.64 \cdot 10^{-6}$		$7.17 \cdot 10^{-8}$	

DOI: 10.1002/jnm

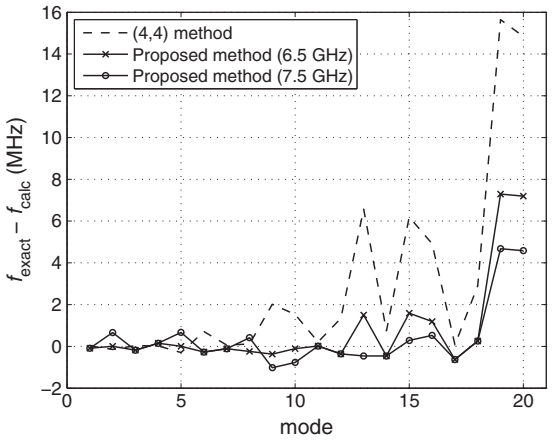

Figure 6. Errors in the calculation of the first 20 resonant frequencies of a 10×10-cm cavity.

5. CONCLUSIONS

With a view to combating inherent flaws of classic FDTD schemes, we have demonstrated the consistent implementation of error-controlling concepts to the development of a high-order algorithm. Starting from a standard (4,4) scheme, conventional operators in space have been replaced by improved ones that amend the corresponding discretization errors isotropically. This alteration has been rendered feasible by first defining an error formula for each approximation and then enforcing the vanishing of leading terms. In addition, a slight modification to the temporal operator yields extra—yet, not strictly narrowband—enhancement at the optimization frequencies. The spectral response of the new algorithm reveals the reliable modeling of high-frequency components, whereas low-frequency errors, although partially deteriorated, do not affect the overall performance decisively. The scheme's theoretical investigation, as well as results from numerical simulations, has shown that fourth-order accuracy is accomplished, which comes as a natural outcome of the proposed nontraditional design of the technique, rather than the usual approach of minimized truncation errors. Overall, the potential and effectiveness of accuracy-preserving FDTD algorithms, suitable for demanding engineering applications, has been illustrated in this paper.

REFERENCES

1. Yee KS. Numerical solution of initial boundary value problems involving Maxwell's equations in isotropic media. *IEEE Transactions on Antennas and Propagation* 1966; **AP-14**:302–307.
2. Taflove A, Hagness SC. *Computational Electrodynamics: The Finite-Difference Time-Domain Method* (3rd edn). Artech House: Boston, MA, 2005.
3. Turkel E. High order methods. In *Advances in Computational Electrodynamics: The Finite-Difference Time-Domain Method*, Taflove A (ed.). Artech House: Boston, MA, 1998; 63–110.
4. Tam CKW, Webb JC. Dispersion-relation-preserving finite difference schemes for computational acoustics. *Journal of Computational Physics* 1993; **107**(2): 262–281.
5. Cole JB. High-accuracy Yee algorithm based on nonstandard finite differences: new developments and verifications. *IEEE Transactions on Antennas and Propagation* 2002; **50**(9):1185–1191.
6. Wang S, Teixeira FL. Dispersion-relation-preserving FDTD algorithms for large-scale three-dimensional problems. *IEEE Transactions on Antennas and Propagation* 2003; **51**(8):1818–1828.
7. Zygiridis TT, Tsiboukis TD. Optimized three-dimensional FDTD discretizations of Maxwell's equations on Cartesian grids. *Journal of Computational Physics* 2007; **226**(2):2372–2388.
8. Tsukerman I. A class of difference schemes with flexible local approximation. *Journal of Computational Physics* 2006; **211**(2): 659–699.
9. Finkelstein B, Kastner R. The spectral order of accuracy: a new unified tool in the design methodology of excitation-adaptive wave equation FDTD schemes. *Journal of Computational Physics* 2009; **228**(24):8958–8984.
10. Kim WT, Koh IS, Yook JG. 3D isotropic dispersion (ID)-FDTD algorithm: update equation and characteristics analysis. *IEEE Transactions on Antennas and Propagation* 2010; **58**(4): 1251–1259.
11. Liu Y, Sen MK. A new time-space domain high-order finite-difference method for the acoustic wave equation. *Journal of Computational Physics* 2009; **228**(23): 8779–8806.
12. Spachmannn H, Schuhmann R, Weiland T. Higher order explicit time integration schemes for Maxwell's equations. *International Journal for Numerical Modelling: Electronic Networks, Devices and Fields* 2002; **15**(5–6):419–437.

DOI: 10.1002/jnm

AUTHOR'S BIOGRAPHY

Theodoros T. Zygiridis received the Diploma and PhD degrees in Electrical and Computer Engineering both from Aristotle University of Thessaloniki, Greece, in 2000 and 2006, respectively. He is currently an appointed lecturer at the Department of Informatics and Telecommunications Engineering, University of Western Macedonia, Greece. His main research interests are in the area of computational electromagnetics and mainly focus on finite-difference time-domain methodologies, high-order techniques, accuracy-preserving algorithms, as well as applications to engineering problems.

DOI: 10.1002/jnm